Article

Optogenetic activation of mGluR1 signaling in the cerebellum induces synaptic plasticity

OPN4
mGluR1a
mCherry

OPN4
mGluR1b
mCherry

Optogenetic Tools

mCherry control

2P

Ca²⁺ Signal
Time

In vitro

LTD

In vivo

AP   Learning
Time

Tatjana Surdin,
Bianca Preissing,
Lennard Rohr, ...,
Stefan Herlitze,
Melanie D. Mark,
Ida Siveke

sxh106@gmail.com (S.H.)
ida.siveke@rub.de (I.S.)

Highlights

Optogenetic tools modulate splice variant-specific mGluR1 signaling

Activation of OPN4-mGluR1 variants induce Gq-mediated intracellular Ca²⁺ increase

Proof-of-concept approach to modulate synaptic plasticity via OPN4-mGluR1a

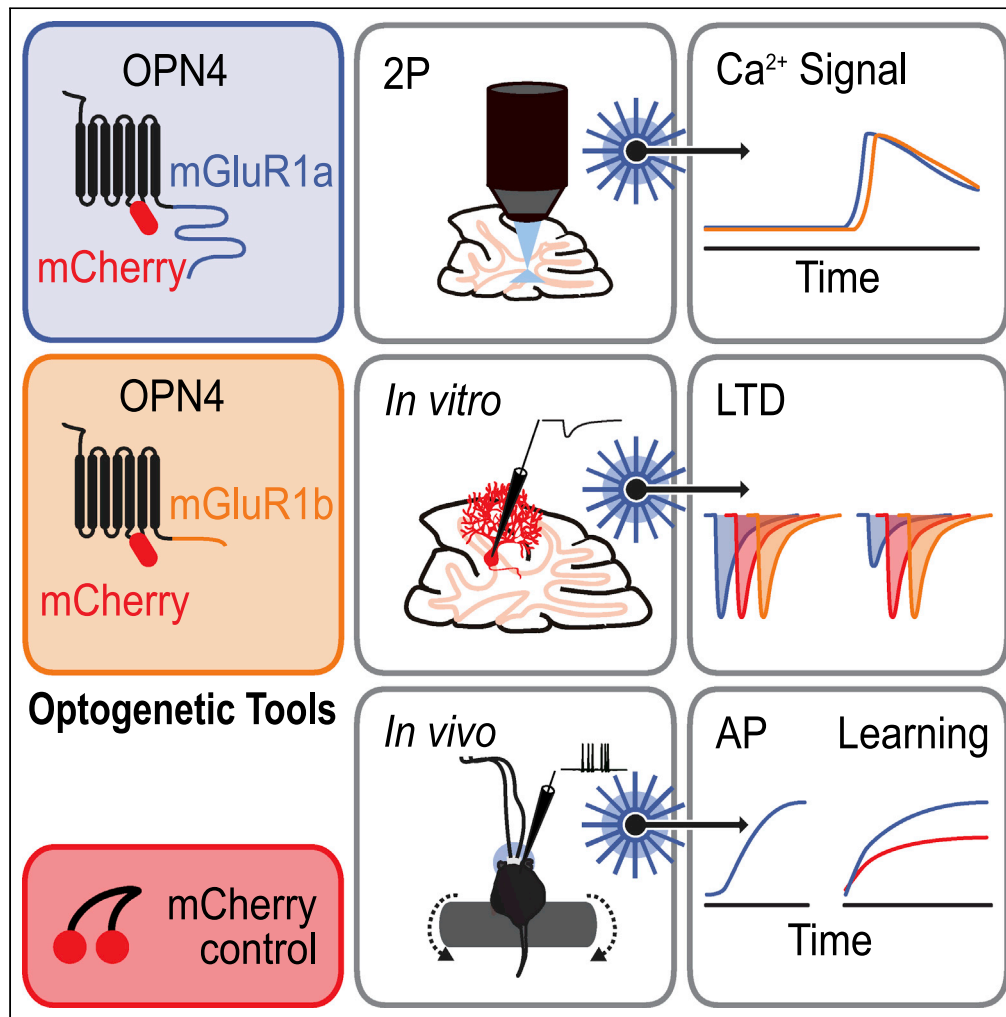OPN4-mGluR1 activation bolsters intrinsic activity and cerebellum driven learning

Article

Optogenetic activation of mGluR1 signaling in the cerebellum induces synaptic plasticity

Tatjana Surdin,[1] Bianca Preissing,[1] Lennard Rohr,[1] Michelle Grömmke,[2] Hanna Böke,[1] Maike Barcik,[3] Zohre Azimi,[4] Dirk Jancke,[4] Stefan Herlitze,[1,*] Melanie D. Mark,[2] and Ida Siveke[1,5,6,*]

SUMMARY

Neuronal plasticity underlying cerebellar learning behavior is strongly associated with type 1 metabotropic glutamate receptor (mGluR1) signaling. Activation of mGluR1 leads to activation of the $G_{q/11}$ pathway, which is involved in inducing synaptic plasticity at the parallel fiber-Purkinje cell synapse (PF-PC) in form of long-term depression (LTD). To optogenetically modulate mGluR1 signaling we fused mouse melanopsin (OPN4) that activates the $G_{q/11}$ pathway to the C-termini of mGluR1 splice variants (OPN4-mGluR1a and OPN4-mGluR1b). Activation of both OPN4-mGluR1 variants showed robust Ca^{2+} increase in HEK cells and PCs of cerebellar slices. We provide the prove-of-concept approach to modulate synaptic plasticity via optogenetic activation of OPN4-mGluR1a inducing LTD at the PF-PC synapse *in vitro*. Moreover, we demonstrate that light activation of mGluR1a signaling pathway by OPN4-mGluR1a in PCs leads to an increase in intrinsic activity of PCs *in vivo* and improved cerebellum driven learning behavior.

INTRODUCTION

Roughly 100,000 parallel fibers (PFs) and one climbing fiber (CF) converge on the dendritic branches of every single Purkinje cell (PC).[1] The simultaneous or mismatched arrival of glutamatergic PF and CF inputs lead to synaptic plasticity at the level of PF-PC synapses.[2] Glutamatergic neurotransmission at the parallel fiber to Purkinje cell synapse is mediated by ionotropic α-amino-3-hydroxy-5-methyl-4-isoxazolepropionic acid receptors (AMPARs) and metabotropic glutamate receptors (mGluRs).

mGluRs belong to the superfamily of G protein coupled receptors (GPCRs), which activate different G protein pathways on a timescale of milliseconds to seconds.[3] Among the mGluR family members, mGluR1 is extensively expressed in PCs, located at the perisynaptic sites of PC dendritic spines in the cerebellar cortex. In contrast to AMPARs, mGluR1s are excluded from postsynaptic density but enriched at perisynaptic sites as well as extrasynaptically.[4–6] High frequency train stimulation of PFs[7,8] or combined CF and PF stimulation[9] activate mGluR1 by glutamate spill over. This induces Gq11-coupled excitatory postsynaptic currents (EPSCs) composed of two components.[10] The first component of the EPSC is mediated by intracellular Ca^{2+} release mobilizing internal Ca^{2+}-stores via activation of inositol 1,4,5-triphosphate (InsP3) receptors.[11] The second component results from DAG dependent activation of canonical nonselective transient receptor potential channel type 3 (TRPC3) producing a slow excitatory postsynaptic potential (EPSP)[12,13] In addition, mGluR1 activation modulates several other pathways leading to inhibition of A-type K^+ channels[14] and boosting of T-type Ca^{2+} channels.[14–16] Subsequently, supralinear intracellular Ca^{2+} concentration and DAG jointly activate PKC and α-Ca^{2+}/calmodulin dependent protein kinase II (αCaMKII).[17] PKC phosphorylates AMPAR subunit GluR2 leading to endocytosis of AMPARs and long-term depression (LTD) of PF-PC synapses.[18,19] The occurrence of the different pathways depends on the membrane potential of the PC and is likely a crucial parameter in determining PF synaptic plasticity.[20,21] Finally, mGluR1 induces endocannabinoid (eCB) signaling that modulates post- and presynaptic plasticity.[22–25]

Encoded by *Grm1*, mGluR1 undergoes alternative splicing, resulting in five isoforms: mGluR1a-e, all differing in the length of their CTD.[26] Of those, mGluR1a and mGluR1b are the predominantly expressed isoforms found in cerebellar PCs.[16] Global knockout (KO) of mGluR1 does not affect cerebellar morphology or basic firing properties of PCs, but leads to severe ataxia, impairments in motor coordination and eyeblink conditioning[27] and impaired LTD at PF-PC synapses.[28] Importantly, behavior impairments and the

[1]Department of Zoology and Neurobiology, Ruhr-University Bochum, Bochum, Germany

[2]Behavioral Neuroscience, Ruhr-University Bochum, Bochum, Germany

[3]Cardiovascular Research Institute Düsseldorf, Division of Cardiology, Pulmonology, and Vascular Medicine, University Duesseldorf, Medical Faculty, Duesseldorf, Germany

[4]Optical Imaging Group, Institut für Neuroinformatik, Ruhr-University Bochum, Bochum, Germany

[5]Bridge Institute of Experimental Tumor Therapy, West German Cancer Center, University Hospital Essen, Essen, Germany

[6]Lead contact

*Correspondence:
sxh106@gmail.com (S.H.),
ida.siveke@rub.de (I.S.)
https://doi.org/10.1016/j.isci.2022.105828

impaired LTD at the PF-PC synapse of mGluR1-KO can be rescued by PC specific expression of mGluR1a but not mGluR1b.[29–31]

Cerebellar disorders resulting from disruption of mGluR1 signaling have been described in a heterogeneous group of autoimmune, neoplastic, and genetic human disorders such as paraneoplastic degeneration (PCD) and spinocerebellar ataxia (SCA).[16] The involvement of mGluR1 in these human diseases has been studied in mouse models. Deletion of mGluR1 in mice causes ataxic gait and motor discoordination as well as impairment of cerebellar driven motor learning including motor impairments and learning deficits on the rotarod.[27,28]

Although compelling evidence shows that mGluR1 is indispensable for normal neuronal plasticity and cerebellar functions, current techniques lack spatiotemporal or activity-dependent precision to resolve modulatory qualities of mGluR1 signaling. To understand neuronal network modulation by GPCRs, various optogenetic and pharmacogenetic approaches have been developed. For optogenetic modulations light-activated GPCRs such as vertebrate rod and cone opsins, parapinopsin, melanopsin and jellyfish opsin have been established to control the $G_{i/o}$, $G_{q/11}$ and G_s pathways, respectively.[32–43] To achieve highly customized GPCR specific targeting and downstream signaling, chimeras of suitable opsins and GPCR domains of choice have been engineered by exchanging the intracellular domains between the light-activated and ligand-gated GPCRs.[39,40,44–46]

Here, we developed an optogenetic chimera by fusing the C-termini of the two predominantly expressed mGluR1 isoforms of PCs, the mGluR1a and mGluR1b, to vertebrate mouse melanopsin carrying mCherry in the third intracellular loop for receptor localization.[33] Activation of the OPN4-mGluR1 variants showed robust Ca^{2+} increase in HEK cells and PCs of cerebellar slices. Moreover, using these chimeric light-activated GPCRs we demonstrate mGluR1a isoform specific modulation of long-term plasticity at the PF-PC synapse *in vitro*, increase in PC spiking activity *in vivo*, and a possible involvement of mGluR1 signaling in cerebellum-driven motor skill learning.

RESULTS

Design and characterization of OPN4-mGluR1 variants

We created two optogenetic tools to control the function of $G_{q/11}$ pathway activation in splice variant specific mGluR1 domains. We used vertebrate mouse melanopsin (OPN4) as a light-activated GPCR for controlling the $G_{q/11}$ pathway.[36] For monitoring the localization of OPN4, mCherry was inserted into the third intracellular loop of OPN4.[33] The mGluR1 C-termini of mGluR1a (long, 355aa) or mGluR1b (short, 67aa) were fused to the C-terminus of OPN4 as neuronal trafficking signals (Figures 1A and 1B). To analyze the $G_{q/11}$ dependent increase in intracellular Ca^{2+} concentration by the optogenetic constructs, we expressed these constructs together with GCaMP6m in HEK293 cells and recorded Ca^{2+} activity over 90 s using 480 nm wavelength for simultaneous imaging and photostimulation (Figure 1C). As indicated in Figure 1D, light-mediated activation of OPN4-mGluR1a and OPN4-mGluR1b induced intracellular Ca^{2+} responses with comparable kinetics (Figure 1F). OPN4-mGluR1a Ca^{2+} responses are similar to pharmacological activation of mGluR1a (Figure 1E, purple) and can be blocked by YM-254890, a $G_{q/11}$-protein inhibitor (Figure 1E, green). Taken together, OPN4-mGluR1 variants were both functional and induced robust Ca^{2+} signals in HEK293 cells mediated by $G_{q/11}$ protein activation.

Examination of functional expression of OPN4-mGluR1 variants using *in vitro* Ca^{2+}- imaging in PCs

To verify the functional expression of OPN4-mGluR1 variants in cerebellar slices OPN4-mGluR1a, OPN4-mGluR1b, or the mCherry control were virally expressed together with GCaMP6m in PCs (Figures 2A, 2E, and 2I). All constructs were expressed at the distal and proximal dendrites and the somata of the PCs (Figures 2B, 2F, and 2J). Light-mediated activation of OPN4-mGluR1a and OPN4-mGluR1b (wavelength 965 nm for photostimulation and imaging) induced elevated Ca^{2+} levels (Figures 2C and 2G). The Ca^{2+} increase initiated at the distal dendrites and traveled from the proximal dendrites to the soma of the PCs. This characteristic activity is reflected in the increased mean time of 2/3 activation of the maximal fluorescence along the PC (Figures 2D and 2H). In contrast, PCs expressing mCherry showed only spontaneous Ca^{2+} activity, but less fluorescence changes at the soma and no spontaneous Ca^{2+} events at the dendrites (Figures 2K and 2L). Thus, both OPN4-mGluR1 variants show robust Ca^{2+} signals in PCs, demonstrating that both optogenetic chimeras are functionally expressed in the cerebellar PCs.
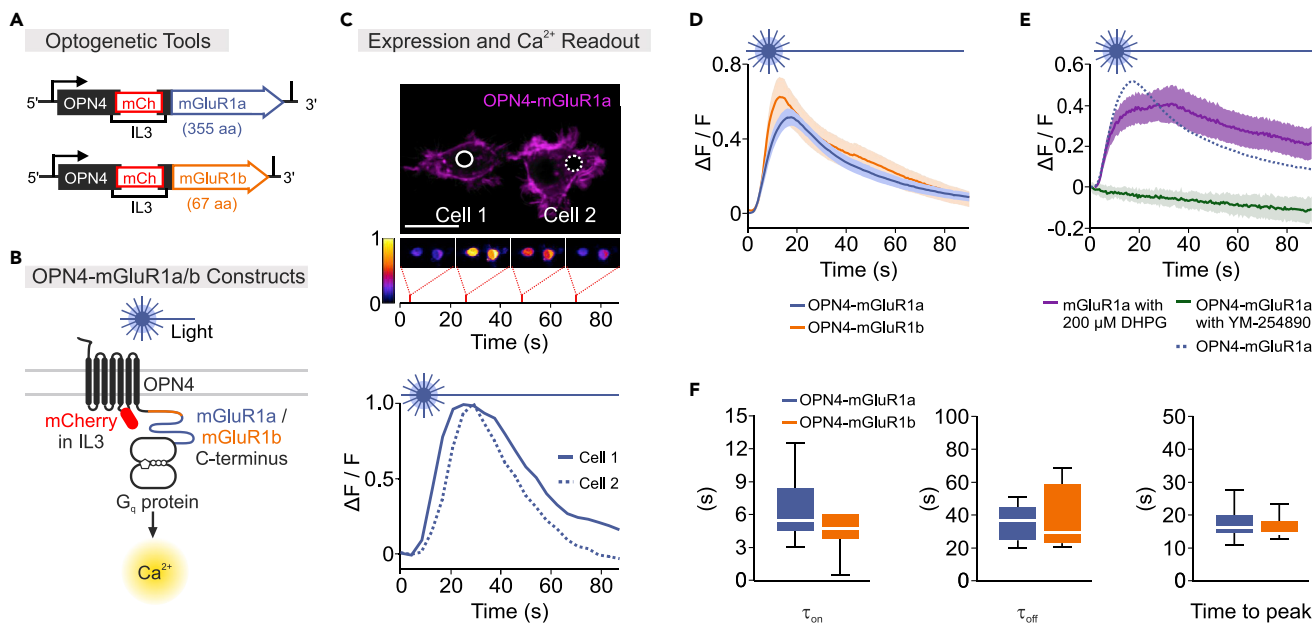
Figure 1. Design and characterization of OPN4-mGluR1 variants

(A) Design of OPN4-mGluR1a (blue) and OPN4-mGluR1b (orange) constructs. Chimeras comprise OPN4, mCherry in the third intracellular loop and mGluR1a or mGluR1b fused c-terminally.

(B) Scheme of OPN4-mGluR1 design and Gq-coupled Ca^{2+} increase following photostimulation.

(C) Top, exemplary OPN4-mGluR1a expression in two HEK293 cells. The construct is localized in the cell membrane. Bottom, transient Ca^{2+} signal of both cells during light stimulation. Scale bar, 10μm.

(D) Time-course of light-activated Ca^{2+} signaling of OPN4-mGluR1a (blue, n = 15 dishes) and OPN4-mGluR1b (orange, n = 8 dishes) over a stimulation period of 90 seconds. Shading indicates ± SEM.

(E) Pharmacological activation of mGluR1a in HEK293 cells shows comparable increase and delayed peak of Ca^{2+} signaling (purple, n = 13 dishes). Pharmacological block of $G_{q/11}$ protein signaling abolishes OPN4-mGluR1a Ca^{2+} signals (green).

(F) Ca^{2+} signal components τ_{on}, τ_{off} and time to peak were compared between optogenetic chimeras and showed no differences. Population data of the responses shown in d are shown as boxplot (mean ± SEM).

Modulation of synaptic plasticity by OPN4-mGluR1 variants *in vitro*

mGluR1 activation is involved in inducing cerebellar LTD. Of interest, in mGluR1-KO mice only mGluR1a but not mGluR1b rescued synaptic LTD at the PF-PC synapse.[30] To explore effects of OPN4-mGluR1 on cerebellar plasticity, both variants - OPN4-mGluR1a and OPN4-mGluR1b (Figures 3B and 3C) - were virally expressed in PCs. For LTD induction, we combined light stimulation (470 nm, pulses 400 ms, 75× at 0.5 Hz) with electrical PF-stimulation (75× at 0.5 Hz). As indicated in Figure 3C III, light stimulation in the presence of OPN4-mGluR1a, but not OPN4-mGluR1b (Figure 3D III) or control mCherry (Figure 3E III) induced robust LTD at the PF-PC synapse.

It has been reported that high Ca^{2+} transients can induce PF-PC LTD.[47] Therefore, we investigated if optogenetic stimulation of OPN4-mGluR1a mediated Ca^{2+} transients alone are sufficient to induce LTD (Figure 4A). However, such stimulation did not induce LTD at the stimulated PF-PC synapse (Figure 4A). Next, we investigated if local PF stimulation is required to induce LTD at the specific PF-PC synapse. We combined global optogenetic activation of OPN4-mGluR1a paired with PC depolarization at the soma (Figure 4B). Such global stimulation did not induce LTD at the PF-PC synapse. However, subsequent application of light combined with PF stimulation (as used in Figure 3) resulted in LTD of the EPSCs (Figure 4C). These data indicate that light-dependent activation of OPN4-mGluR1a only in conjunction with local PF stimulation is sufficient to induce long-term plasticity in form of LTD at the PF-PC synapse.

Modulation of Purkinje cell simple spikes by OPN4-mGluR1a *in vivo*

mGluR1 also modulates the intrinsic simple spike firing frequency of cerebellar PCs. We next investigated whether OPN4-mGluR1a modulates the intrinsic firing activity of PCs *in vivo* (Figure 5A). Application of mGluR1 agonist (DHPG) as well as light-pulse stimulation increased simple spike firing frequency (Figures 5B and 5C).
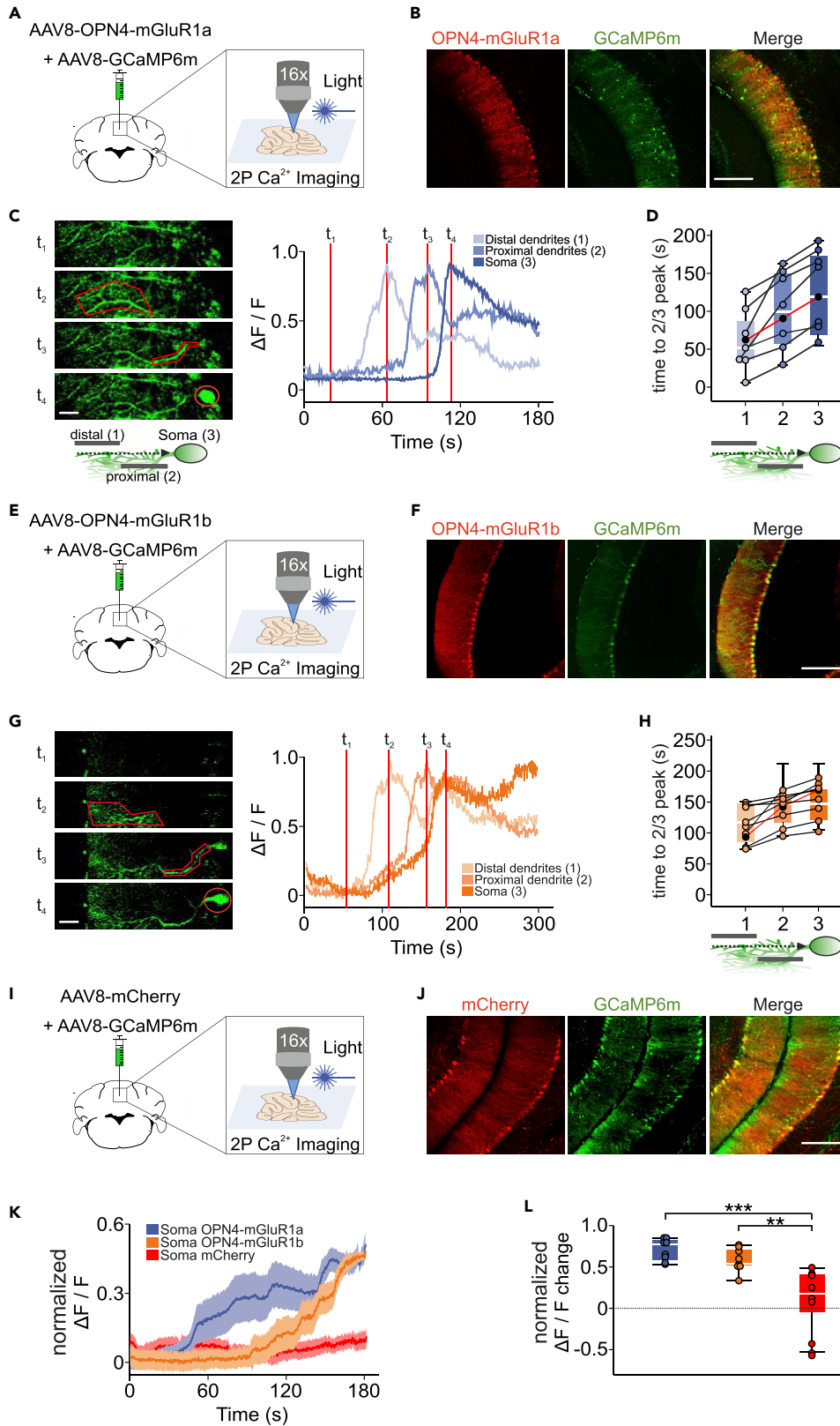
A AAV8-OPN4-mGluR1a
+ AAV8-GCaMP6m

B OPN4-mGluR1a · GCaMP6m · Merge

C

distal (1) · Soma (3)
proximal (2)

D

E AAV8-OPN4-mGluR1b
+ AAV8-GCaMP6m

F OPN4-mGluR1b · GCaMP6m · Merge

G

H

I AAV8-mCherry
+ AAV8-GCaMP6m

J mCherry · GCaMP6m · Merge

K

L

Figure 2. Functional assessment of OPN4-mGluR1 Variants by *in vitro* Ca^{2+}-Imaging in PCs

(A, E, and I) Scheme of experimental procedure for the 2-photon imaging *in vitro* and expression of OPN4-mGluR1a.

(B) OPN4-mGluR1b.

(F and J) or mCherry (J) together with GCaMP6m in the PC of cerebellar slices. Scale bar, 120μm.

(C and G) Exemplary transient Ca^{2+} signal during light stimulation. Time-course of light-activated Ca^{2+} increase by OPN4-mGluR1a (C, right) or OPN4-mGluR1b (G, right) at the soma, the proximal and distal dendrite. Scale bar, 25μm.

(D and H) Population data of the time to 2/3 peak at the different regions are shown as boxplot (mean ± SEM).

(K) Time-course of mean light-activated Ca^{2+} signaling of the respective constructs at the soma (OPN4-mGluR1a: n = 8; OPN4-mGluR1b: n = 9; mCherry: n = 10). Lines indicate the means, shading ±SEM.

(L) Population data of the responses shown in k are shown as boxplot (mean ± SEM). Maximal fluorescence changes are compared between optogenetic chimeras and the mCherry-control and showed statistically significant differences (Kruskal-Wallis test; p < 0.0001; 1a/mCherry, p < 0.0001; 1b/mCherry, p = 0.015).

OPN4-mGluR1a Activation in Active Cerebellar Region Promotes Procedural Learning

mGluR1a and cerebellar LTD are important for motor learning.[1] Global loss of mGluR1 leads to motor impairment, which can be rescued by selective expression of mGluR1a/b in cerebellar PCs.[30] We screened for regions of the cerebellum that are active during motor learning on the accelerated rotarod using the Fos-TRAP mouseline[48] crossed with LSL-tdTomato mice. In these mice, 4-hydroxy-tamoxifen (4-OHT)-dependent Cre recombinase is expressed under control of the c-Fos promoter, allowing cre-mediated recombination and identification of active tdTomato positive neurons following 4-OHT administration (Figure 6A). Rotarod experiments were performed followed by 4-OHT injection 30 min after the last trial (Figures 6B and 6C) to reach a timed overlay of early gene c-Fos expression by the task and maximal 4-OHT presence. Mice successfully learned to balance on the accelerating rotarod (Figure 6D). Comparison of active regions between rotarod and home-cage littermates (Figure 6E) revealed significantly lower activity in lobules VI and X, simple lobule (SIM), and crus 2 of the ansiform lobule (Crus II) (Figure 6F, grey). In cerebellar lobule VIII and copula of the pyramid (COP) activity was significantly upregulated during rotarod (Figure 6F, red).

Therefore, to modulate mGluR1 signaling in previous identified active cerebellar regions, we expressed OPN4-mGluR1a or mCherry (as control) in pcp2-cre mice (Figure 6G) in the lobule VIII. To investigate motor learning, mice underwent training sessions for two consecutive days on the accelerated rotarod. After the first trial without stimulation, mice received continuous photo-stimulation during the time on the rotarod for all consecutive trials (Figure 6H). Motor performance and learning rate of OPN4-mGluR1a mice in comparison to mCherry controls did not reveal differences at D1 of acquisition, but the learning rate increased for OPN4-mGluR1a compared to mCherry expressing mice at D2 (Figures 6I and 6J). Performance in starting trials (without photo-stimulation) did not differ between groups (Figure 6K) indicating equal basic performance.

In summary, electrophysiological results and behavioral experiments suggest that light-activation of the G$_{q/11}$ pathway in mGluR1a receptor domains by OPN4-mGluR1a mediates long-term synaptic plasticity in cerebellar PCs and modulates cerebellum-driven motor learning.

DISCUSSION

We designed an optogenetic GPCR, OPN4-mGluR1a, to control mGluR1a signaling domains in cells. Our results show that optogenetic stimulation of OPN4-mGluR1 activates G$_{q/11}$ protein signaling cascades. OPN4-mGluR1a, but not OPN4-mGluR1b induced LTD of evoked EPSCs at the PF-PC synapse in cerebellar PCs *in vitro*. *In vivo* single cell recordings verify that light activation of OPN4-mGluR1a and pharmacological activation of mGluR1 signaling by the mGluR1 agonist DHPG increased spontaneous neuronal activity. Finally, procedural learning assessment suggests activation of OPN4-mGluR1a in cerebellar regions involved in rotarod performance improve learning of the rotarod task without changing the basic behavioral performance.

It has been proposed that LTD induced by coincident PF and CF activation is a critical component of cerebellar learning. More recent studies promote the critical role of mGluR1 in LTD induction in the cerebellum and hippocampus.[49–52] These *in vitro* studies demonstrate that mGluR1 agonist DHPG induced LTD-like persistent reduction of hippocampal and of cerebellar PF to PC synaptic transmission. We now established a method to control the mGluR1 signaling pathway optogenetically. We show that light-dependent activation of OPN4-mGluR1a, but not OPN4-mGluR1b induces LTD at the PF-PC synapse. This result suggests that splice variant dependent-targeting of OPN4 is important for anchoring the construct at synaptic sites, at which LTD occurs. In addition, we discovered *in vivo* that OPN4-mGluR1a increase spontaneous simple
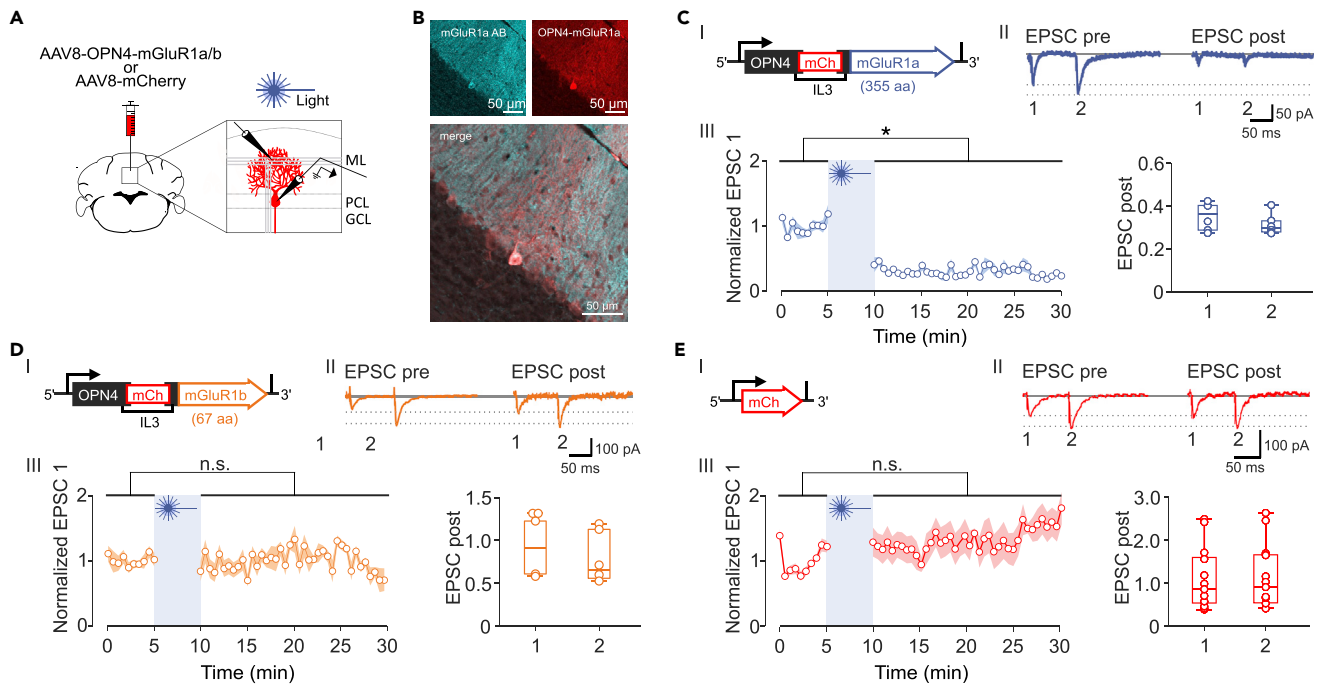
Figure 3. Activation of OPN4-mGluR1a but not OPN4-mGluR1b induced LTD in cerebellar Purkinje cell recordings *in vitro*

(A) Scheme of experimental procedure for cerebellar slice recordings. OPN4-mGluR1a, OPN4-mGluR1b or mCherry were expressed in Purkinje cells using AAVs.

(B) Expression pattern of OPN4-mGluR1a in PCs; mGluR1a antibody (cyan) and OPN4-mGluR1a (red), colocalization (white).

(C–E) EPSCs were evoked by double pulse stimulation of parallel fibers combined with 470 blue light stimulation of OPN4-mGluR1a (c; n = 6), OPN4-mGluR1b (d; n = 6) and mCherry-control (e; n = 11). I Design of OPN4-mGluR1a (blue), OPN4-mGluR1b (orange) and mCherry (red) constructs. Chimeras comprise OPN4, mCherry in the third intracellular loop and mGluR1a or mGluR1b fused c-terminally. II Example traces of EPSCs are shown on the top, III shows the normalized EPSC1. EPSCs were normalized to the average pre-EPSC (0–5 min). Response of the EPSCs before and after blue light stimulation is given as mean response over time (pre: 0–5 min; post: 10–30 min). Significant LTD of post EPSCs (p = 0.031; two-sided Wilcoxon signed-rank test) was only induced by optical stimulation of OPN4-mGluR1a.

spike firing comparable to native mGluR1 activation by DHPG. These findings are in line with published *in vitro* and *in vivo* studies showing that application of mGluR1 agonists such as DHPG enhances the simple spike rate of PCs in current clamp and extracellular recordings.[53–55]

We demonstrated that light-dependent activation of OPN4-mGluR1a expressed in PCs induces an increase in spontaneous firing and synaptic depression at the PF-PC synapse. It has been shown that mGluR1 contributes to the basal activity of PCs, where mGluR1 activation induces an inward cation current and an increase in spiking of PCs *in vitro* and *in vivo*[56] We hypothesize that light-dependent activation of OPN4-mGluR1a induces a cation current leading to a depolarization increasing intrinsic firing of PCs *in vivo*. The critical link between the mGluR1 dependent depolarization and the observed LTD at the PF-PC synapse is most likely TRPC3.[12] This channel is abundantly expressed in cerebellar PCs and responsible for the mGluR-mediated slow EPSCs.[12] Another possibility is that an InsP3-induced Ca^{2+} release from Ca^{2+} stores may contribute to increased intrinsic firing in PCs. However, increased intracellular Ca^{2+} levels in PCs also activate Ca^{2+}-activated K^+ channels leading to a hyperpolarization instead of a depolarization of PCs.[57] This hyperpolarization would lead to a decrease in intrinsic firing of the PCs. Therefore, which specific downstream pathway and what contribution of these pathways regulates the optogenetically induced mGluR1-mediated increase in PC firing has to be further investigated. Our studies reveal that OPN4-mGluR1 allows the photoswitchable control of the $G_{q/11}$ protein pathway leading to increased neuronal activity, and precise regulation of synaptic plasticity in a subcellular localization-dependent manner.

Theoretical work by Marr and Albus hypothesizes that PF-PC LTD in the cerebellum implements motor learning.[58,59] This hypothesis has been supported by the experimental data of Ito and colleagues
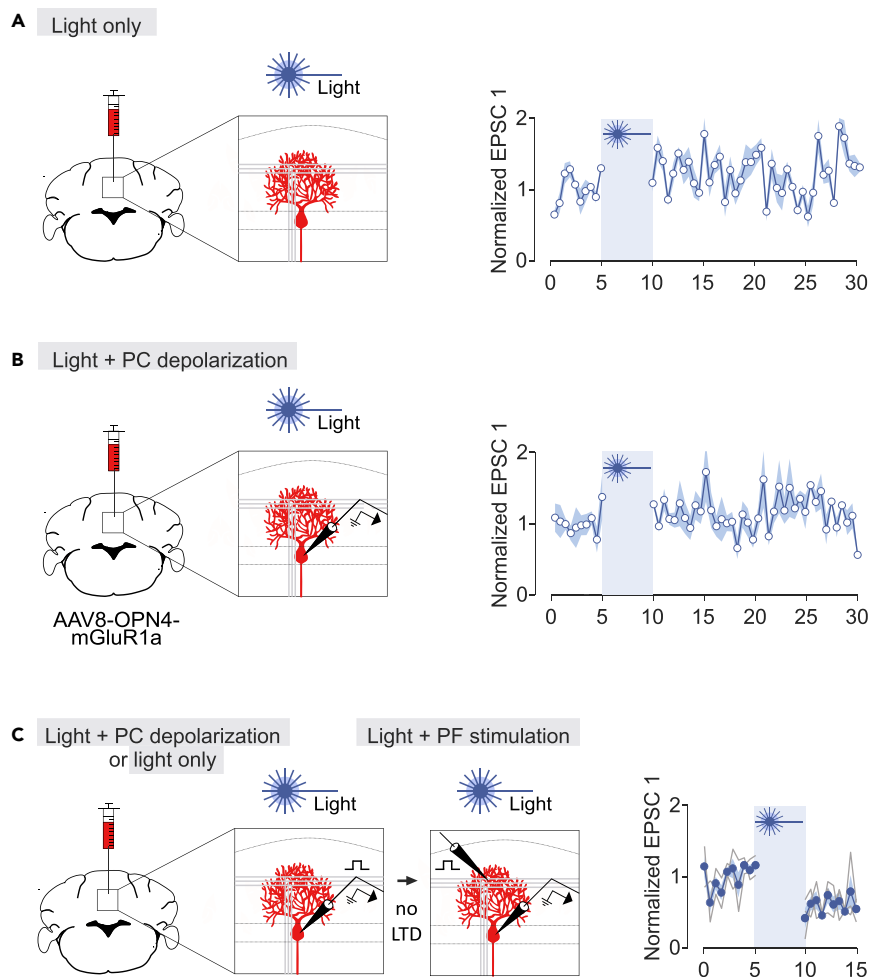
Figure 4. Different stimulation protocols for OPN4-mGluR1a induced LTD

(A–C) Scheme of experimental procedure for the different protocols to induce LTD in cerebellar slice recordings are shown on the left. OPN4-mGluR1a was expressed in PCs using AAVs. EPSCs were evoked by double pulse stimulation of PFs before and after optical 470 blue light (470 nm), stimulation alone (A, n = 3) or blue light (470 nm) stimulation combined with PC depolarization (from −60 to −10 mV) (B; n = 4). These two protocols did not induce LTD, however, subsequent application of light combined with PF stimulation resulted in LTD of the EPSC (Figure 5C; n = 3).

forming the basic concept of cerebellar learning. Cerebellar learning requires cerebellar plasticity and involves various synapses within the cerebellar neuronal network. Cerebellar plasticity depends for example on the composition and spatial distribution of different channels and receptors, local concentrations of Ca^{2+} and nitric oxide and the timing of the incoming inputs.[60] However, there is a long-standing debate whether an increase or decrease in synaptic strength at the PF-PC synapse underlies motor learning. For example, it has been shown that mice deficient in cerebellar LTD have no effects in rotarod task.[61,62] Other studies using mutant mouse lines with deficits in LTD and LTP inductions argue that LTP rather than LTD may the key mechanism for cerebellar motor learning.[63,64] Recent studies using optogenetic control of synaptic AMPA receptor endocytosis strengthened the idea that LTD in the cerebellum is responsible for motor learning underlying adaptation of the optokinetic response and vestibulo-ocular reflex.[65] Another strong correlation between cerebellar LTD induction and motor coordination has been found in mGluR1-deficient mice. These mice show impairments in LTD in the cerebellum and deficits in several behavior motor tasks including rotarod performance. In a subsequent study Ichise et al. showed that although mGluR1 deficient mice failed on the rotarod, mGluR1 rescue mice showed normal LTD and normal motor behavior.[29] The role of mGluR1 signaling for motor behavior could further be shown in $G_{q/11}$ protein deficient mice that had no cerebellar LTD and were significantly impaired on motor behavior including the rotating rod.[66] We show that light-dependent activation protocols of $G_{q/11}$
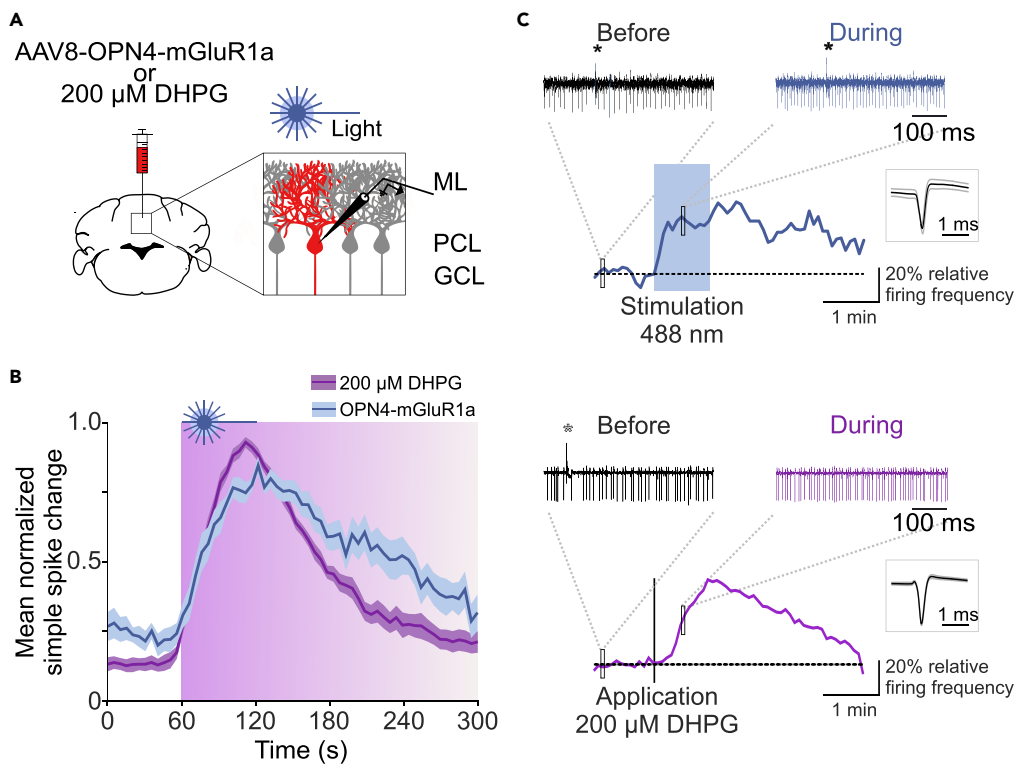
Figure 5. OPN4-mGluR1a elevates Purkinje cell simple spike firing rate *in vivo*

(A) Scheme of experimental procedure for single-cell recordings in cerebellum in anesthetized mice. Recordings were made two weeks after AAV8-OPN4-mGluR1a injection, DHPG was locally applied during recordings.

(B) Pharmacological activation of mGluR1 (DHPG - mGluR1 agonist, purple trace) or blue light activation OPN4-mGluR1a (488 nm; blue trace) lead to a rise in simple spike firing frequency (DHPG: n = 30 PCs in n = 3 mice; OPN4-mGluR1a: n = 12 PCs in n = 4 mice). Lines indicate the means, shading ±SEM.

(C) Exemplary Purkinje cell recordings (identified by characteristic simple and complex spike firing pattern, marked with *) over 5 min with 60 s baseline recoding and subsequent optogenetic activation using 488 nm wavelength (top) or pharmacological activation (DHPG - mGluR1 agonist, bottom).

signals in mGluR1 GPCR-domains in cerebellar PCs, which induce LTD *in vitro*, improve learning performance on the rotarod. Thus, our data support the correlation between LTD induction at the PF-PC synapse and enhanced motor learning. However, many other mechanisms, signaling pathways and plasticity events throughout the cerebellar network involving various cell-types and synapses act in synergy to encode cerebellum driven motor learning.[67,68]

Several human disorders such as PCD and SCA have been associated with pathological changes of mGluR1 signaling induced by autoimmune, neoplastic and genetic dysregulations.[1,16,69] Pharmacological treatment that enhances mGluR1 signaling using positive allosteric modulators resulted in a significant long-lasting improvement of motor performance in the SCA mouse model.[44] On the other hand, mGluR1-negative allosteric modulator rescued moderate ataxia in an early SCA1 mouse model.[70] The underlying temporal and spatial mechanism are still under debate. However, the evidence that hypofunction and hyperfunction of mGluR1 signaling underlies certain types of human SCAs[16] suggests modulation of mGluR1 signaling, as a promising therapeutic target for cerebellar ataxic diseases. Thus, our new optogenetic tool OPN4-mGluR1a, opens new possibilities to study and treat different types of cerebellar diseases such as SCA or PCD.

Limitations of the study

In our study, we developed an optogenetic approach for splice-variant specific activation of mGluR1 signaling in the cerebellum. We tested the basic function of our designed tools by Ca^{2+} imaging in HEK cells and cerebellar slices. Gq/11 mediated changes in intracellular Ca^{2+} signals are only one of
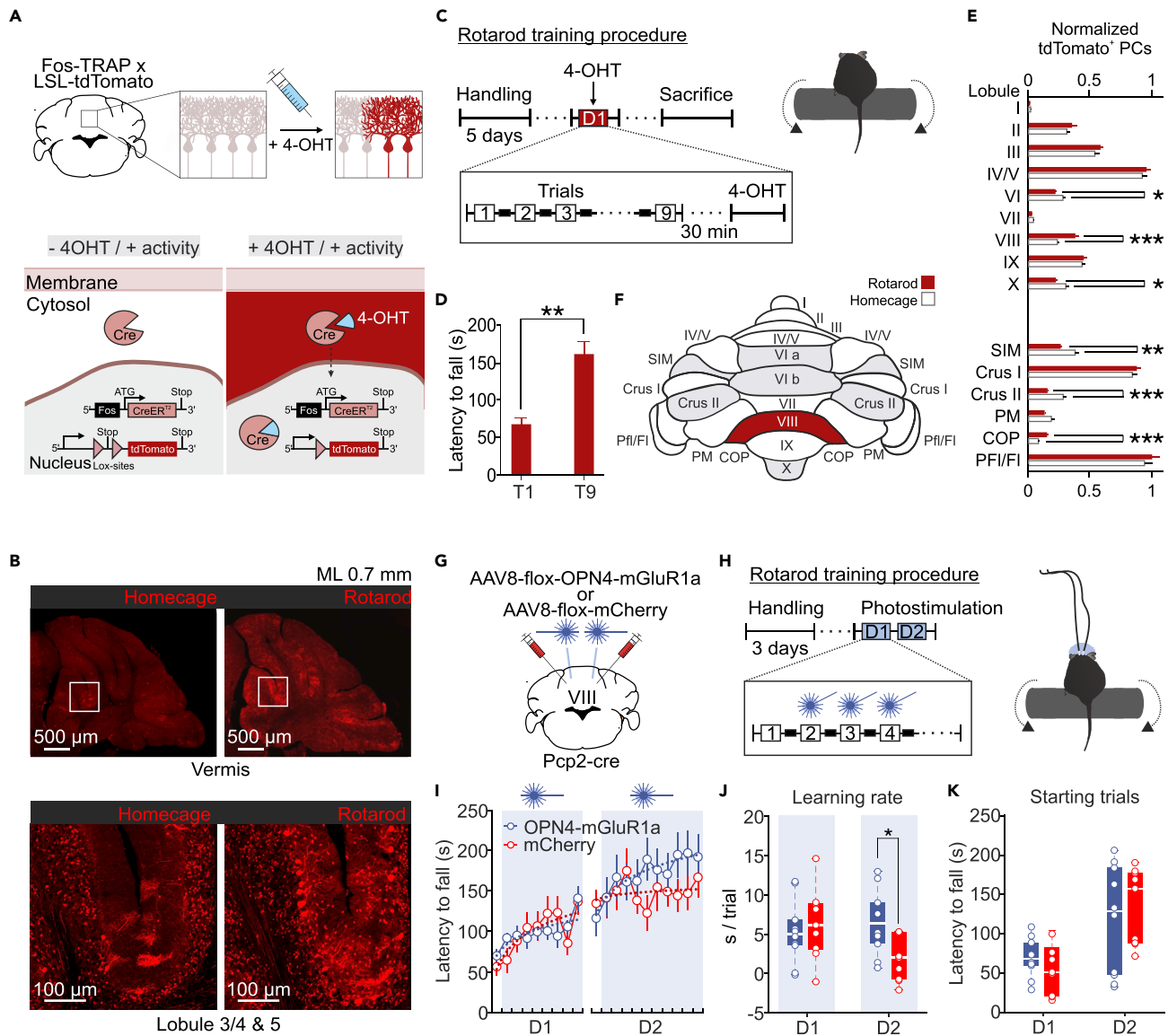
Figure 6. OPN4-mGluR1a Activation in Active Cerebellar Region Promotes Procedural Learning

(A) Schematic drawing showing induction of tdTomato expression by active cells in Fos-TRAP x LSL-tdTomato mouse line. Neuronal activation induces expression of immediate early gene c-Fos. CreER^{T2} is expressed under c-Fos promoter but is retained in the cytoplasm when 4-OHT is absent. Upon injection of 4-OHT, CreER^{T2} enters the nucleus, excises the STOP-cassette and enables tdTomato expression.

(B) Exemplary expression patterns of control and rotarod trained mice. Bottom, cerebellar lobes 3, 4 and 5 are shown magnified.

(C) Protocol for rotarod training and 4-OHT injection 30 min after completion of the last trial.

(D) Motor learning indicated by elevated latency to fall on accelerating rotarod (mean +SEM; t_{11} = −4.37, p = 0.001; n = 12 trained mice).

(E) tdTomato$^+$ Purkinje cells in cerebellar areas of rotarod trained and homecage mice (rotarod-trained, n = 12; homecage, n = 12 mice).

(F) Summary of cerebellar areas with different tdTomato$^+$ Purkinje cells (grey decrease, red increase; lobe IV, t_{22} = −2.59, p = 0.017; lobe lobe VIII, t_{22} = 5.182, p < 0.001; lobe X, t_{22} = −2.712, p = 0.013; Sim, $t_{14.375}$ = −3.498, p = 0.003; CrusII, $t_{12.67}$ = −4.748, p < 0.001; COP, t_{22} = 5.874, p < 0.001).

(G) OPN4-mGluR1a (n = 9) or mCherry (n = 9) were injected into cerebellar vermis lobe VIII and light guides were implanted.

(H) Rotarod training protocol consisted of two days (D1 & D2) with optogenetic stimulation during rotarod sessions. One training session consisted of 9 trials on D1 and 11 trials on D2. Optical stimulation started at trial 2 on both days.

(I) Performance (measured as latency to fall) increases with training on D1 and D2 (mean ± SEM).

(J) Learning rates of OPN4-mGluR1a expressing mice on D2 are significantly higher after photostimulation (p = 0.028, Mann-Whitney U test).

(K) Performance did not differ between groups on starting trials of both days (without stimulation).

several targets of mGluR1 signaling. Therefore, we cannot exclude the possibility that OPN4-mGluR1 variants activate all different mGluR1 signaling targets. We also do not know how long-term activation and exogenous expression of OPN4-mGluR1 affect gene transcription and PC morphology. However, we did not observe obvious physiological or morphological changes of PCs. Furthermore, by optogenetic stimulation of our OPN4-mGluR1a tool we induced LTD at the PF-PC synapse *in vitro* and a behavior effect *in vivo*, that is described to underlie cerebellar learning. However, the relationship between these two findings is speculative and a functional *in vivo* study including pharmacological experiments would be necessary to prove the causal link between the synaptic changes measured *in vitro* and the behavior findings.

STAR★METHODS

Detailed methods are provided in the online version of this paper and include the following:

- KEY RESOURCES TABLE
- RESOURCE AVAILABILITY
  - Lead contacts
  - Materials cvailability
  - Data and code availability
- EXPERIMENTAL MODEL AND SUBJECT DETAILS
- METHOD DETAILS
  - Generation of plasmid constructs
  - Cell culture and life cell confocal imaging
  - Viral vector production
  - Surgery, virus injections and optic fibre implantation
  - Slicing and *in vitro* slice recordings
  - *In vitro* Ca^{2+} imaging in cerebellar slices
  - Extracellular *in vivo* electrophysiological recordings in anaesthetized mice
  - Immunohistochemistry
  - Behavioral paradigms
  - Behavioral labeling using 4-hydrotamoxifen
- QUANTIFICATION AND STATISTICAL ANALYSIS

SUPPLEMENTAL INFORMATION

Supplemental information can be found online at https://doi.org/10.1016/j.isci.2022.105828.

AUTHOR CONTRIBUTIONS

Conceptualization, T.S., S.H., and I.S.; Methodology and Investigation, T.S., B.P., L.R., M.G., H.B., M.B., and I.S.; Data analysis, T.S., L.R., Z.A., and I.S.; Funding acquisition, D.J., S.H., and M.D.M.; Supervision, D.J., S.H., M.D.M, and I.S.; Writing, T.S., S.H., and I.S.

DECLARATION OF INTERESTS

The authors declare no competing interests.

REFERENCES

1. Kano, M., Hashimoto, K., and Tabata, T. (2008). Type-1 metabotropic glutamate receptor in cerebellar Purkinje cells: a key molecule responsible for long-term depression, endocannabinoid signalling and synapse elimination. Philos. Trans. R. Soc. Lond. B Biol. Sci. 363, 2173–2186. https://doi.org/10.1098/rstb.2008.2270.

2. Zang, Y., and De Schutter, E. (2019). Climbing fibers provide graded error signals in cerebellar learning. Front. Syst. Neurosci. 13, 46. https://doi.org/10.3389/fnsys.2019.00046.

3. Reiner, A., and Levitz, J. (2018). Glutamatergic signaling in the central nervous system: ionotropic and metabotropic receptors in concert. Neuron 98, 1080–1098. https://doi.org/10.1016/j.neuron.2018.05.018.

4. Baude, A., Nusser, Z., Roberts, J.D., McIlhinney, R.A., Mulvihill, E., and Somogyi, P. (1993). The metabotropic glutamate receptor (mGluRIα) is concentrated at perisynaptic membrane of neuronal subpopulations as detected by immunogold reaction. Neuron 11, 771–787. https://doi.org/10.1016/0896-6273(93)90086-7.

5. Nusser, Z., Mulvihill, E., Streit, P., and Somogyi, P. (1994). Subsynaptic segregation of metabotropic and ionotropic glutamate receptors as revealed by immunogold localization. Neuroscience 61, 421–427. https://doi.org/10.1016/0306-4522(94)90421-9.

6. Lujan, R., Nusser, Z., Roberts, J.D., Shigemoto, R., and Somogyi, P. (1996). Perisynaptic location of metabotropic glutamate receptors mGluR1 and mGluR5 on dendrites and dendritic spines in the rat hippocampus. Eur. J. Neurosci. 8, 1488–1500. https://doi.org/10.1111/j.1460-9568.1996.tb01611.x.

7. Batchelor, A.M., and Garthwaite, J. (1997). Frequency detection and temporally dispersed synaptic signal association through a metabotropic glutamate receptor pathway. Nature 385, 74–77. https://doi.org/10.1038/385074a0.

8. Tempia, F., Alojado, M.E., Strata, P., and Knöpfel, T. (2001). Characterization of the mGluR(1)-mediated electrical and calcium signaling in Purkinje cells of mouse cerebellar slices. J. Neurophysiol. 86, 1389–1397. https://doi.org/10.1152/jn.2001.86.3.1389.

9. Dzubay, J.A., and Otis, T.S. (2002). Climbing fiber activation of metabotropic glutamate receptors on cerebellar Purkinje neurons. Neuron 36, 1159–1167. https://doi.org/10.1016/s0896-6273(02)01052-8.

10. Batchelor, A.M., and Garthwaite, J. (1993). Novel synaptic potentials in cerebellar Purkenje cells: probable mediation by metabotropic glutamate receptors. Neuropharmacology 32, 11–20. https://doi.org/10.1016/0028-3908(93)90124-L.

11. Takechi, H., Eilers, J., and Konnerth, A. (1998). A new class of synaptic response involving calcium release in dendritic spines. Nature 396, 757–760. https://doi.org/10.1038/25547.

12. Hartmann, J., Dragicevic, E., Adelsberger, H., Henning, H.A., Sumser, M., Abramowitz, J., Blum, R., Dietrich, A., Freichel, M., Flockerzi, V., et al. (2008). TRPC3 channels are required for synaptic transmission and motor coordination. Neuron 59, 392–398. https://doi.org/10.1016/j.neuron.2008.06.009.

13. Venkatachalam, K., and Montell, C. (2007). TRP channels. Annu. Rev. Biochem. 76, 387–417. https://doi.org/10.1146/annurev.biochem.75.103004.142819.

14. Otsu, Y., Marcaggi, P., Feltz, A., Isope, P., Kollo, M., Nusser, Z., Mathieu, B., Kano, M., Tsujita, M., Sakimura, K., and Dieudonné, S. (2014). Activity-dependent gating of calcium spikes by A-type K+ channels controls climbing fiber signaling in Purkinje cell dendrites. Neuron 84, 137–151. https://doi.org/10.1016/j.neuron.2014.08.035.

15. Hildebrand, M.E., Isope, P., Miyazaki, T., Nakaya, T., Garcia, E., Feltz, A., Schneider, T., Hescheler, J., Kano, M., Sakimura, K., et al. (2009). Functional coupling between mGluR1 and Cav3.1 T-type calcium channels contributes to parallel fiber-induced fast calcium signaling within Purkinje cell dendritic spines. J. Neurosci. 29, 9668–9682. https://doi.org/10.1523/JNEUROSCI.0362-09.2009.

16. Yamasaki, M., Aiba, A., Kano, M., and Watanabe, M. (2021). mGluR1 signaling in cerebellar Purkinje cells: subcellular organization and involvement in cerebellar function and disease. Neuropharmacology 194, 108629. https://doi.org/10.1016/j.neuropharm.2021.108629.

17. Jörntell, H., and Hansel, C. (2006). Synaptic memories upside down: bidirectional plasticity at cerebellar parallel fiber-Purkinje cell synapses. Neuron 52, 227–238. https://doi.org/10.1016/j.neuron.2006.09.032.

18. Matsuda, S., Launey, T., Mikawa, S., and Hirai, H. (2000). Disruption of AMPA receptor GluR2 clusters following long-term depression induction in cerebellar Purkinje neurons. EMBO J. 19, 2765–2774. https://doi.org/10.1093/emboj/19.12.2765.

19. Xiao, M.-Y., Zhou, Q., and Nicoll, R.A. (2001). Metabotropic glutamate receptor activation causes a rapid redistribution of AMPA receptors. Neuropharmacology 41, 664–671. https://doi.org/10.1016/S0028-3908(01)00134-4.

20. Ait Ouares, K., Filipis, L., Tzilivaki, A., Poirazi, P., and Canepari, M. (2019). Two distinct sets of Ca2+ and K+ channels are activated at different membrane potentials by the climbing fiber synaptic potential in Purkinje neuron dendrites. J. Neurosci. 39, 1969–1981. https://doi.org/10.1523/JNEUROSCI.2155-18.2018.

21. Ait Ouares, K., and Canepari, M. (2020). The origin of physiological local mGluR1 supralinear Ca2+ signals in cerebellar Purkinje neurons. J. Neurosci. 40, 1795–1809. https://doi.org/10.1523/JNEUROSCI.2406-19.2020.

22. Maejima, T., Hashimoto, K., Yoshida, T., Aiba, A., and Kano, M. (2001). Presynaptic inhibition caused by retrograde signal from metabotropic glutamate to cannabinoid receptors. Neuron 31, 463–475. https://doi.org/10.1016/S0896-6273(01)00375-0.

23. Safo, P.K., and Regehr, W.G. (2005). Endocannabinoids control the induction of cerebellar LTD. Neuron 48, 647–659. https://doi.org/10.1016/j.neuron.2005.09.020.

24. Qiu, D.-L., and Knöpfel, T. (2009). Presynaptically expressed long-term depression at cerebellar parallel fiber synapses. Pflügers Archiv 457, 865–875. https://doi.org/10.1007/s00424-008-0555-9.

25. Kano, M., Ohno-Shosaku, T., Hashimotodani, Y., Uchigashima, M., and Watanabe, M. (2009). Endocannabinoid-mediated control of synaptic transmission. Physiol. Rev. 89, 309–380. https://doi.org/10.1152/physrev.00019.2008.

26. Ferraguti, F., Crepaldi, L., and Nicoletti, F. (2008). Metabotropic glutamate 1 receptor: current concepts and perspectives. Pharmacol. Rev. 60, 536–581. https://doi.org/10.1124/pr.108.000166.

27. Aiba, A., Kano, M., Chen, C., Stanton, M.E., Fox, G.D., Herrup, K., Zwingman, T.A., and Tonegawa, S. (1994). Deficient cerebellar long-term depression and impaired motor learning in mGluR1 mutant mice. Cell 79, 377–388.

28. Conquet, F., Bashir, Z.I., Davies, C.H., Daniel, H., Ferraguti, F., Bordi, F., Franz-Bacon, K., Reggiani, A., Matarese, V., and Condé, F. (1994). Motor deficit and impairment of synaptic plasticity in mice lacking mGluR1. Nature 372, 237–243. https://doi.org/10.1038/372237a0.

29. Ichise, T., Kano, M., Hashimoto, K., Yanagihara, D., Nakao, K., Shigemoto, R., Katsuki, M., and Aiba, A. (2000). mGluR1 in cerebellar Purkinje cells essential for long-term depression, synapse elimination, and motor coordination. Science 288, 1832–1835. https://doi.org/10.1126/science.288.5472.1832.

30. Ohtani, Y., Miyata, M., Hashimoto, K., Tabata, T., Kishimoto, Y., Fukaya, M., Kase, D., Kassai, H., Nakao, K., Hirata, T., et al. (2014). The synaptic targeting of mGluR1 by its carboxyl-terminal domain is crucial for cerebellar function. J. Neurosci. 34, 2702–2712. https://doi.org/10.1523/JNEUROSCI.3542-13.2014.

31. Kishimoto, Y., Fujimichi, R., Araishi, K., Kawahara, S., Kano, M., Aiba, A., and Kirino, Y. (2002). mGluR1 in cerebellar Purkinje cells is required for normal association of temporally contiguous stimuli in classical conditioning. Eur. J. Neurosci. 16, 2416–2424. https://doi.org/10.1046/j.1460-9568.2002.02407.x.

32. Bailes, H.J., Zhuang, L.-Y., and Lucas, R.J. (2012). Reproducible and sustained

regulation of Gαs signalling using a metazoan opsin as an optogenetic tool. PLoS One *7*, e30774. https://doi.org/10.1371/journal.pone.0030774.

33. Eickelbeck, D., Karapinar, R., Jack, A., Suess, S.T., Barzan, R., Azimi, Z., Surdin, T., Grömmke, M., Mark, M.D., Gerwert, K., et al. (2019). CaMello-XR enables visualization and optogenetic control of Gq/11 signals and receptor trafficking in GPCR-specific domains. Commun. Biol. *2*, 60. https://doi.org/10.1038/s42003-019-0292-y.

34. Li, X., Gutierrez, D.V., Hanson, M.G., Han, J., Mark, M.D., Chiel, H., Hegemann, P., Landmesser, L.T., and Herlitze, S. (2005). Fast noninvasive activation and inhibition of neural and network activity by vertebrate rhodopsin and green algae channelrhodopsin. Proc. Natl. Acad. Sci. USA *102*, 17816–17821. https://doi.org/10.1073/pnas.0509030102.

35. Masseck, O.A., Spoida, K., Dalkara, D., Maejima, T., Rubelowski, J.M., Wallhorn, L., Deneris, E.S., and Herlitze, S. (2014). Vertebrate cone opsins enable sustained and highly sensitive rapid control of Gi/o signaling in anxiety circuitry. Neuron *81*, 1263–1273. https://doi.org/10.1016/j.neuron.2014.01.041.

36. Spoida, K., Eickelbeck, D., Karapinar, R., Eckhardt, T., Mark, M.D., Jancke, D., Ehinger, B.V., König, P., Dalkara, D., Herlitze, S., and Masseck, O.A. (2016). Melanopsin variants as intrinsic optogenetic on and off switches for transient versus sustained activation of G protein pathways. Curr. Biol. *26*, 1206–1212. https://doi.org/10.1016/j.cub.2016.03.007.

37. Wagdi, A., Malan, D., Sathyanarayanan, U., Beauchamp, J.S., Vogt, M., Zipf, D., Beiert, T., Mansuroglu, B., Dusend, V., Meininghaus, M., et al. (2022). Selective optogenetic control of Gq signaling using human Neuropsin. Nat. Commun. *13*, 1765. https://doi.org/10.1038/s41467-022-29265-w.

38. Copits, B.A., Gowrishankar, R., O'Neill, P.R., Li, J.N., Girven, K.S., Yoo, J.J., Meshik, X., Parker, K.E., Spangler, S.M., Elerding, A.J., et al. (2021). A photoswitchable GPCR-based opsin for presynaptic inhibition. Neuron *109*, 1791–1809.e11. https://doi.org/10.1016/j.neuron.2021.04.026.

39. van Wyk, M., Pielecka-Fortuna, J., Löwel, S., and Kleinlogel, S. (2015). Restoring the ONswitch in blind retinas: opto-mGluR6, a next-generation, cell-tailored optogenetic tool. PLoS Biol. *13*, e1002143. https://doi.org/10.1371/journal.pbio.1002143.

40. Spangler, S.M., and Bruchas, M.R. (2017). Optogenetic approaches for dissecting neuromodulation and GPCR signaling in neural circuits. Curr. Opin. Pharmacol. *32*, 56–70. https://doi.org/10.1016/j.coph.2016.11.001.

41. Alagarsamy, S., Saugstad, J., Warren, L., Mansuy, I.M., Gereau, R.W., and Conn, P.J. (2005). NMDA-induced potentiation of mGluR5 is mediated by activation of protein phosphatase 2B/calcineurin. Neuropharmacology *49*, 135–145. https://doi.org/10.1016/j.neuropharm.2005.05.005.

42. Dai, R., Yu, T., Weng, D., Li, H., Cui, Y., Wu, Z., Guo, Q., Zou, H., Wu, W., Gao, X., et al. (2022). A neuropsin-based optogenetic tool for precise control of Gq signaling. Sci. China Life Sci. *65*, 1271–1284. https://doi.org/10.1007/s11427-022-2122-0.

43. Mahn, M., Saraf-Sinik, I., Patil, P., Pulin, M., Bitton, E., Karalis, N., Bruentgens, F., Palgi, S., Gat, A., Dine, J., et al. (2021). Efficient optogenetic silencing of neurotransmitter release with a mosquito rhodopsin. Neuron *109*, 1621–1635.e8. https://doi.org/10.1016/j.neuron.2021.03.013.

44. Airan, R.D., Thompson, K.R., Fenno, L.E., Bernstein, H., and Deisseroth, K. (2009). Temporally precise in vivo control of intracellular signalling. Nature *458*, 1025–1029. https://doi.org/10.1038/nature07926.

45. Oh, E., Maejima, T., Liu, C., Deneris, E., and Herlitze, S. (2010). Substitution of 5-HT1A receptor signaling by a light-activated G protein-coupled receptor. J. Biol. Chem. *285*, 30825–30836. https://doi.org/10.1074/jbc.M110.147298.

46. Spoida, K., Masseck, O.A., Deneris, E.S., and Herlitze, S. (2014). Gq/5-HT2c receptor signals activate a local GABAergic inhibitory feedback circuit to modulate serotonergic firing and anxiety in mice. Proc. Natl. Acad. Sci. USA *111*, 6479–6484. https://doi.org/10.1073/pnas.1321576111.

47. Hartell, N.A. (1996). Strong activation of parallel fibers produces localized calcium transients and a form of LTD that spreads to distant synapses. Neuron *16*, 601–610. https://doi.org/10.1016/S0896-6273(00)80079-3.

48. Guenthner, C.J., Miyamichi, K., Yang, H.H., Heller, H.C., and Luo, L. (2013). Permanent genetic access to transiently active neurons via TRAP: targeted recombination in active populations. Neuron *78*, 773–784. https://doi.org/10.1016/j.neuron.2013.03.025.

49. Kano, M., and Watanabe, T. (2017). Type-1 metabotropic glutamate receptor signaling in cerebellar Purkinje cells in health and disease. F1000Res. *6*, 416. https://doi.org/10.12688/f1000research.10485.1.

50. Palmer, M.J., Irving, A.J., Seabrook, G.R., Jane, D.E., and Collingridge, G.L. (1997). The group I mGlu receptor agonist DHPG induces a novel form of LTD in the CA1 region of the hippocampus. Neuropharmacology *36*, 1517–1532. https://doi.org/10.1016/S0028-3908(97)00181-0.

51. Huber, K.M., Kayser, M.S., and Bear, M.F. (2000). Role for rapid dendritic protein synthesis in hippocampal mGluR-dependent long-term depression. Science *288*, 1254–1257. https://doi.org/10.1126/science.288.5469.1254.

52. Sdrulla, A.D., and Linden, D.J. (2007). Double dissociation between long-term depression and dendritic spine morphology in cerebellar Purkinje cells. Nat. Neurosci. *10*, 546–548. https://doi.org/10.1038/nn1889.

53. Lingenhöhl, K., Knöpfel, T., and Olpe, H.-R. (1993). Multiphasic responses of cerebellar Purkinje cells to 1S, 3R-ACPD: an in vivo study. Neurosci. Res. *18*, 223–228. https://doi.org/10.1016/0168-0102(93)90057-W.

54. Yamakawa, Y., and Hirano, T. (1999). Contribution of mGluR1 to the basal activity of a mouse cerebellar Purkinje neuron. Neurosci. Lett. *277*, 103–106. https://doi.org/10.1016/S0304-3940(99)00852-6.

55. Yuan, Q., Qiu, D.-L., Weber, J.T., Hansel, C., and Knöpfel, T. (2007). Climbing fiber-triggered metabotropic slow potentials enhance dendritic calcium transients and simple spike firing in cerebellar Purkinje cells. Mol. Cell. Neurosci. *35*, 596–603. https://doi.org/10.1016/j.mcn.2007.05.004.

56. Knöpfel, T., and Grandes, P. (2002). Metabotropic glutamate receptors in the cerebellum with a focus on their function in Purkinje cells. Cerebellum *1*, 19–26. https://doi.org/10.1007/BF02941886.

57. Canepari, M., and Ogden, D. (2006). Kinetic, pharmacological and activity-dependent separation of two Ca2+ signalling pathways mediated by type 1 metabotropic glutamate receptors in rat Purkinje neurones. J. Physiol. *573*, 65–82. https://doi.org/10.1113/jphysiol.2005.103770.

58. Albus, J.S. (1971). A theory of cerebellar function. Math. Biosci. *10*, 25–61. https://doi.org/10.1016/0025-5564(71)90051-4.

59. Ito, M. (1989). Long-term depression. Annu. Rev. Neurosci. *12*, 85–102. https://doi.org/10.1146/annurev.ne.12.030189.000505.

60. De Zeeuw, C.I., Lisberger, S.G., and Raymond, J.L. (2021). Diversity and dynamism in the cerebellum. Nat. Neurosci. *24*, 160–167. https://doi.org/10.1038/s41593-020-00754-9.

61. Burguière, E., Arleo, A., Hojjati, M.R., Elgersma, Y., De Zeeuw, C.I., Berthoz, A., and Rondi-Reig, L. (2005). Spatial navigation impairment in mice lacking cerebellar LTD: a motor adaptation deficit? Nat. Neurosci. *8*, 1292–1294. https://doi.org/10.1038/nn1532.

62. Lefort, J.M., Rochefort, C., and Rondi-Reig, L.; Group of L.R.R. is member of Bio-Psy Labex and ENP Foundation (2015). Cerebellar contribution to spatial navigation: new insights into potential mechanisms. Cerebellum *14*, 59–62. https://doi.org/10.1007/s12311-015-0653-0.

63. Schonewille, M., Belmeguenai, A., Koekkoek, S.K., Houtman, S.H., Boele, H.J., van Beugen, B.J., Gao, Z., Badura, A., Ohtsuki, G., Amerika, W.E., et al. (2010). Purkinje cell-specific knockout of the protein phosphatase PP2B impairs potentiation and cerebellar motor learning. Neuron *67*, 618–628. https://doi.org/10.1016/j.neuron.2010.07.009.

64. Schonewille, M., Gao, Z., Boele, H.J., Veloz, M.F.V., Amerika, W.E., Simek, A.A.M., De Jeu, M.T., Steinberg, J.P., Takamiya, K., Hoebeek, F.E., et al. (2011). Reevaluating the role of LTD in cerebellar motor learning. Neuron *70*, 43–50. https://doi.org/10.1016/j.neuron.2011.02.044.

65. Kakegawa, W., Katoh, A., Narumi, S., Miura, E., Motohashi, J., Takahashi, A., Kohda, K., Fukazawa, Y., Yuzaki, M., and Matsuda, S. (2018). Optogenetic control of synaptic AMPA receptor endocytosis reveals roles of LTD in motor learning. Neuron 99, 985–998.e6. https://doi.org/10.1016/j.neuron.2018.07.034.

66. Hartmann, J., Blum, R., Kovalchuk, Y., Adelsberger, H., Kuner, R., Durand, G.M., Miyata, M., Kano, M., Offermanns, S., and Konnerth, A. (2004). Distinct roles of Galpha(q) and Galpha11 for Purkinje cell signaling and motor behavior. J. Neurosci. 24, 5119–5130. https://doi.org/10.1523/JNEUROSCI.4193-03.2004.

67. Gao, Z., van Beugen, B.J., and De Zeeuw, C.I. (2012). Distributed synergistic plasticity and cerebellar learning. Nat. Rev. Neurosci. 13, 619–635. https://doi.org/10.1038/nrn3312.

68. Johansson, F. (2019). Intrinsic memory of temporal intervals in cerebellar Purkinje cells. Neurobiol. Learn. Mem. 166, 107103. https://doi.org/10.1016/j.nlm.2019.107103.

69. Edfawy, M., Guedes, J.R., Pereira, M.I., Laranjo, M., Carvalho, M.J., Gao, X., Ferreira, P.A., Caldeira, G., Franco, L.O., Wang, D., et al. (2019). Abnormal mGluR-mediated synaptic plasticity and autism-like behaviours in Gprasp2 mutant mice. Nat. Commun. 10, 1431. https://doi.org/10.1038/s41467-019-09382-9.

70. Power, E.M., Morales, A., and Empson, R.M. (2016). Prolonged type 1 metabotropic glutamate receptor dependent synaptic signaling contributes to spino-cerebellar ataxia type 1. J. Neurosci. 36, 4910–4916. https://doi.org/10.1523/JNEUROSCI.3953-15.2016.

71. Rudyk, C., Dwyer, Z., McNeill, J., Salmaso, N., Farmer, K., Prowse, N., and Hayley, S. (2019). Chronic unpredictable stress influenced the behavioral but not the neurodegenerative impact of paraquat. Neurobiol. Stress 11, 100179. https://doi.org/10.1016/j.ynstr.2019.100179.

72. Tye, K.M., Mirzabekov, J.J., Warden, M.R., Ferenczi, E.A., Tsai, H.C., Finkelstein, J., Kim, S.Y., Adhikari, A., Thompson, K.R., Andalman, A.S., et al. (2013). Dopamine neurons modulate neural encoding and expression of depression-related behaviour. Nature 493, 537–541. https://doi.org/10.1038/nature11740.

73. Beyer, H.M., Gonschorek, P., Samodelov, S.L., Meier, M., Weber, W., and Zurbriggen, M.D. (2015). AQUA cloning: a versatile and simple enzyme-free cloning approach. PLoS One 10, e0137652. https://doi.org/10.1371/journal.pone.0137652.

74. Choi, J.H., Yu, N.K., Baek, G.C., Bakes, J., Seo, D., Nam, H.J., Baek, S.H., Lim, C.S., Lee, Y.S., and Kaang, B.K. (2014). Optimization of AAV expression cassettes to improve packaging capacity and transgene expression in neurons. Mol. Brain 7, 17. https://doi.org/10.1186/1756-6606-7-17.

75. Kroeze, W.K., Sassano, M.F., Huang, X.P., Lansu, K., McCorvy, J.D., Giguère, P.M., Sciaky, N., and Roth, B.L. (2015). PRESTO-Tango as an open-source resource for interrogation of the druggable human GPCRome. Nat. Struct. Mol. Biol. 22, 362–369. https://doi.org/10.1038/nsmb.3014.

76. Hirata, H., Takahashi, A., Shimoda, Y., and Koide, T. (2016). Caspr3-Deficient mice exhibit low motor learning during the early phase of the accelerated rotarod task. PLoS One 11, e0147887. https://doi.org/10.1371/journal.pone.0147887.

77. Ye, L., Allen, W.E., Thompson, K.R., Tian, Q., Hsueh, B., Ramakrishnan, C., Wang, A.C., Jennings, J.H., Adhikari, A., Halpern, C.H., et al. (2016). Wiring and molecular features of prefrontal ensembles representing distinct experiences. Cell 165, 1776–1788. https://doi.org/10.1016/j.cell.2016.05.010.

STAR★METHODS

KEY RESOURCES TABLE

REAGENT or RESOURCE	SOURCE	IDENTIFIER
Antibodies		
Rabbit anti mGluR1a	Sigma-Aldrich	Cat# G9665; RRID: AB_259995
Bacterial and virus strains		
Stellar Competent Cells	TaKaRa	Cat# 636763
AAV8-OPN4-mGluR1a	This paper	N/A
AAV8-OPN4-mGluR1b	This paper	N/A
AAV8-mCherry	This paper	N/A
AAV8-flox-OPN4-mGluR1a	This paper	N/A
AAV8-flox-GCaMP6m	This paper	N/A
AAV8-flox-mCherry	This paper	N/A
Chemicals, peptides, and recombinant proteins		
QX314 chloride	Tocris Bioscience	CAS# 5369-03-9
Picrotoxin	Sigma-Aldrich	CAS# 124-87-8
9-cis-Retinal	Sigma-Aldrich	CAS# 514-85-2
Polyethylenimine (PEI)	Polysciences	Cat# 23966
(R,S)-3,5-DHPG, group I mGlu receptor agonist	Abcam	CAS# 19641-83-9
4-hydroxytamoxifen(4-OHT)	Sigma-Aldrich	CAS# 68392-35-8
Experimental models: Cell lines		
HEK293-T cells	Dr. Deniz Dalkara	N/A
Experimental models: Organisms/strains		
Mouse: C57Bl/6	The Jackson Laboratory	RRID:IMSR_JAX:000664
Mouse: Pcp2(L7)-cre/B6.129-Tg(Pcp2-cre)2Mpin/J	The Jackson Laboratory	RRID:IMSR_JAX:004146
Mouse: Fos-TRAP/B6.129(Cg)-$Fos^{tm1.1(cre/ERT2)Luo}$/J	The Jackson Laboratory	RRID:IMSR_JAX:021882
Mouse: B6.Cg-$Gt(ROSA)$ $26Sor^{tm14(CAG-tdTomato)Hze}$/J	The Jackson Laboratory	RRID:IMSR_JAX:007914
Oligonucleotides		
See Table S1 - Primerlist		
Recombinant DNA		
pAAV-CMV-mGluR1a-IRES-GCaMP6m	This paper	N/A
pAAV-CMV-mGluR1a-p2A-GCaMP6m	This paper	N/A
GRM1-Tango	Addgene	Plasmid #66387
pAAV-CMV-flox-GCaMP6m	This paper	N/A
pAAV-CMV-OPN4-mGluR1a-CT	This paper	N/A
pAAV-CMV-OPN4-mGluR1b-CT	This paper	N/A
pAAV-CMV-flox-OPN4-mGluR1a-CT	This paper	N/A
pGP-CMV-GCaMP6m	Addgene	Plasmid #40754
pAAV-EF1a-mCherry	This paper	N/A
pAAV-EF1a-flox-mCherry	This paper	N/A

Continued

REAGENT or RESOURCE	SOURCE	IDENTIFIER
Software and algorithms		
MATLAB	Mathworks	https://www.mathworks.com/products/matlab.html
Patchmaster software	HEKA	https://www.heka.com/
Sigma Plot	Systat software	http://www.systat.de/
FIJI (ImageJ)	ImageJ	https://imagej.net/software/fiji/downloads

RESOURCE AVAILABILITY

Lead contacts

Stefan Herlitze (sxh106@gmail.com) and Ida Siveke (ida.siveke@rub.de).

Materials cvailability

The commercially available material is denoted in the manuscript. Further information and requests for resources and reagents should be directed to and will be fulfilled by the lead contacts Stefan Herlitze or Ida Siveke.

Commercially available material is denoted in the manuscript and the key resources table.

Data and code availability

- The datasets will be shared by the lead contact upon request.

- All codes that were used for analysis are available upon reasonable request from the lead contacts.

- Any additional information required to reanalyze the data reported in this paper is available from the lead contact upon request

EXPERIMENTAL MODEL AND SUBJECT DETAILS

All experiments were conducted with approval of a local ethics committee (Bezirksamt Arnsberg) and the animal care committee of Nordrhein-Westfalen (LANUV; Landesamt für Umweltschutz, Naturschutz und Verbraucherschutz Nordrhein-Westfalen, Germany; AZ. 84-02.04.2014.A203 und AZ.81-02.04.2019.A228). The study was carried out in accordance with the European Communities Council Directive of 2010 (2010/63/EU) for care of laboratory animals and supervised by the animal welfare commission of the Ruhr-University Bochum. Experiments were performed in 2- to 10-month-old male and female mice of the following lines: C57Bl6/J, homozygous Pcp2-Cre. For c-Fos labeling experiments, heterozygous Fos-CreER^{T2} mice were obtained by crossing wild-type C57BL6/J x Fos-CreER$^{T2 (+/-)}$ mice. Fos-CreER$^{T2 (+/-)}$ and Gt(ROSA)26Sor$^{tm9(CAG-tdTomato)Hze}$/J $^{(+/+)}$ mice were crossed to generate Fos-CreER$^{T2 (+/-)}$ x Gt(ROSA)26Sor$^{tm9(CAG-tdTomato)Hze}$/J $^{(+/-)}$ mice (mouse line is abbreviated as Fos-TRAP hereafter). For *in vitro* and behavioral experiments, age matched animals received viral injections with OPN4-mGLuR1a, OPN4-mGluR1b (only for *in vitro* studies) or mCherry (as control). Mice were kept on a 12/12 day/night cycle with water and food *ad libitum*. To increase the dynamic range of motor learning abilities, the basic motor performance on the rotarod was decreased by application of an adapted mild stress protocol.[71,72] Two days before and during the first two acquisition days on the rotarod, the day/night cycle was changed, and mice were kept on dark cycle for 48 h.

METHOD DETAILS

Generation of plasmid constructs

Plasmids were based on the pAAV-CMV-eGFP-CW3SL vector (GenBank: KJ411916.2) to expand AAV packaging capacity.[73,74] Constructs were generated using the In-Fusion cloning kit (Takara) by PCR amplifying each element with 15 bp overhangs. For generation of pAAV-CMV-mOPN4L-mChil3-CW3SL, the sequence of mCherry was integrated in the third intracellular loop of the long isoform of mouse melanopsin (mOPN4L, GenBank: NM_013887.2). For OPN4-mGluR1a (pAAV-CMV-mOPN4L-mChil3-mGluR1_alpha_CT-CW3SL) the sequence of human mGluR1 alpha C-terminus (amino acids K841-L1194) was fused to pAAV-CMV-mOPN4L-mChil3. For OPN4-mGluR1b (pAAV-CMV-mOPN4L-mChil3-mGluR1_beta_CT-CW3SL) the sequence of

human mGluR1 beta C-terminus (amino acids K841-L906) was fused to mOPN4L-mChil3. Conditional constructs were generated by inversion of the gene of interest and adding flanking pairs of Lox2272 and LoxP sites on 5′ and -3′ end of the gene. To generate the full-length receptor fused to a genetically encoded Ca^{2+} sensor, pAAV-CMV-mGluR1-IRES-GCaMP6m-CW3SL and pAAV-CMV-mGluR1-p2A-GCaMP6m-CW3SL were generated by fusing the mGluR1 sequence from GRM1-Tango – a gift from Bryan Roth (Addgene plasmid #66387; http://n2t.net/addgene:66387; RRID:Addgene_66387;[75]) to an internal ribosome entry site (IRES) or the short p2A sequence and GCaMP6m - a gift from Douglas Kim & GENIE Project (Addgene plasmid # 40754 ; http://n2t.net/addgene:40754 ; RRID:Addgene_40754).

Cell culture and life cell confocal imaging

For *in vitro* imaging experiments, HEK293T cells were cultured on 35 mm glass-bottom dishes and transfected via polyethyleneimine (PEI; Polysciences). Cell imaging was performed using a 20X/0.7NA objective on an inverted Leica TCS SP5 confocal laser scanning microscope, 512 × 512 pixels with ∼0.5 s interval between frames. Cells were detected by their membrane-localized mCherry fluorescent reporter tag using 561 nm DPSS laser. To measure Ca^{2+} responses of optogenetic tools, fluorescence change of GCaMP6m was monitored using 476 and 495 nm argon laser lines, thereby simultaneously activating the opsin-based constructs. To measure Ca^{2+} responses of the full-length receptor, 200μM (R,S)-3,5-dihydroxyphenylglycine (DHPG; Abcam) was applied to the dishes. Changes in fluorescence intensity were processed using the time series analyzer V3 function in Fiji and the responses calculated as $\frac{F(t) - \overline{F}_{baseline}}{\overline{F}_{baseline}}$ over time, where $\overline{F}_{baseline}$ is the mean fluorescence of the first two frames of each session.

Viral vector production

Recombinant AAV2/8 genomes were produced using the AAV helper-free system (Agilent Technologies, Santa Clara, CA) by triple transfection of HEK tsA201 cells. Adeno-associated virus (AAV) plasmids encoding the respective gene of interest, the helper plasmid encoding AAV *rep* and *cap* genes, as well as adenoviral helper plasmid were co-transfected into HEK tsA201 cells using polyethyleneimine (PEI). Following ∼72 h incubation, cells were harvested and lysed by 5–7 freeze-thaw cycles while the supernatant was incubated with 40% PEG-8000 for 2 hat 4°C on a shaker. After centrifugation at 3700 × g for 20 minat 4°C, the pellet resulting from PEG-precipitation was resuspended with the supernatant from cell lysate. To purify the AAV, the buffer was replaced with 50 mM HEPES buffer using PEG-precipitation and chloroform added (1:1 ratio). The mixture was thoroughly vortexed for 2 min and centrifuged at 370 × g for 5 min. The resulting aqueous phase was collected, sterile filtered (0.22 μm syringe filter membrane), PEG-precipitated for 2 h, centrifuged at 3700 × g for 20 min and reconstituted in 0.001% PBS-Pluronic F68. Aliquots were stored at −80°C.

Surgery, virus injections and optic fibre implantation

For surgeries, mice were anesthetized with an initial dose of 5% isoflurane in 1.1 L min^{-1} air flow. Anesthetized mice were placed in a stereotaxic frame (Narishige, Japan) on a heating pad for body temperature maintenance (1.3–2.0% Isoflurane maintenance, adjusted according to breathing rate and pinch reflex). For analgesia, carprofen (2 mg/kg) and buprenorphine (0.1 mg/kg) were administered subcutaneously. In addition, lidocaine was administered under the scalp for local anesthesia. The scalp was shaved and cleaned with 70% ethanol. After incision, the skull was cleaned using saline and 70% ethanol. For virus injections, viruses were drawn up into micropipettes generated by pulling capillaries using a Sutter puller. Three craniotomies were made over the cerebellar vermis and 1 μL of AAV was injected using pressure injection (1st and 2nd: AP = −7.2; ML = ±1; DV = 2–3; 3rd: AP = −7,2; ML = 0; DV = 3). For optogenetic stimulation in behavioral tests, in addition, two custom-made optical fibres (ferrule outer diameter 1.25 mm, with a fibre diameter of 200 μm, 0.39 NA, FT200MT; Thorlabs, Dortmund, Germany) were lowered to 0.8 mm with an angle of 10 degrees in the left and right craniotomy and fixed using Charisma (Heraeus Kulzer, Hanau, Germany), followed by dental cement mixed with black powder. After surgery, mice were housed individually and were allowed to recover for at least 7 days before performing electrophysiological or behavioral experiments.

Slicing and *in vitro* slice recordings

Experiments were performed in darkness. Acute cerebellar slices (250 μm thickness) were prepared from the vermis (sagittal sectioning using a Vibratome VT1000S, Leica) of mice 7–14 days after AAV injection using a dissection solution containing (in mM): 87 NaCl, 2.5 KCl, 0,5 $CaCl_2$, 7 $MgCl_2$, 1.25 NaH_2PO_4,

25 NaHCO$_3$, 10 D-Glucose and 75 Sucrose bubbled with 95% O$_2$ and 5% CO$_2$). Slices were incubated in recording solution (in mM: 125 NaCl, 2.5 KCl, 2 CaCl$_2$, 1 MgSO$_4$, 1.25 NaH$_2$PO$_4$, 26 NaHCO$_3$, and 20 D-Glucose, bubbled with 95% O$_2$ and 5% CO$_2$) at 37°C for 45–60 min and then kept at room temperature. For EPSC recordings, slices were preincubated for 20 min in recording solution containing 25 μM 9-cis-retinal, 0.025% (±)-α-tocopherol (Sigma), 0.2% essentially fatty acid free albumin from bovine serum (BSA, Sigma-Aldrich), and 100μM Picrotoxin (Sigma-Aldrich) to block GABA$_A$R-mediated inhibitory inputs. Internal solution consisted of (in mM): 125 Potassium Gluconate, 10 HEPES, 4 NaCl, 2 MgCl$_2$, 0.2 EGTA, 4 Mg-ATP, 0.4 Na-GTP, and 10 Tris-Phosphocreatine and 5 lidocaine N-ethyl bromide (QX-314; Tocris Bioscience) to block Na$^+$ currents (pH 7.3, 280mOsm). Patch pipette resistance was 3–5 MΩ. PCs were visually identified using 40 X objective attached to an upright microscope (BX51WI, Olympus) that was equipped with infrared illumination and a Polychrome V (TILL Photonics). Using 560 nm wavelength for excitation of mCherry, flashing light pulses (light intensity 1.6 mW/mm^2) were utilized to identify expressing PCs. Whole-cell recordings were performed at 20 kHz and low pass-filtered at 3 kHz using a EPSC10 amplifier (HEKA). PCs were voltage clamped at −60 mV and PF stimuli were applied through a second borosilicate glass pipette filled with recording solution and placed in the molecular cell layer. The measurement consisted of three phases: (1) a baseline pre-LTD-induction recording, (2) LTD induction, and (3) post LTD-induction measurement. For (1) and (3), EPSCs were evoked by paired pulse stimulation of PF (ISI = 100 ms) every 30 s for 5 min pre and 15 min post LTD-induction. To induce LTD (2), 470 nm light pulses (1.8 mW/mm^2) with a duration of 400 ms was presented alone (I), combined with 75 single pulse PF stimulation at 0.5 Hz (II) or combined with a depolarization step of the holding potential from −60 to −10 mV (III). PatchMaster software (HEKA) was used for data acquisition and MATLAB for offline analysis. Recordings that showed failures and no EPSC current upon stimulation were excluded from the LTD analysis (maximal 2 traces per LTD-protocol).

In vitro Ca^{2+} imaging in cerebellar slices

Cerebellar slices were incubated (1 h, 37°C) and 2-Photon (Bruker) Ca^{2+} imaging performed in 25 μM 9-cis Retinal external solution using the 16× objective with 1,6× optical zoom. Expression was checked by laser activation with 1100 nm (OPN4-mGluR1a/b, mCherry; PMT3, Bruker) before and 965 nm (GCamP6m; PMT3, Bruker) after the measurements. To exclude ongoing activation by the 1100 nm laser, slices were incubated for 10 min in darkness before imaging. Ca^{2+} imaging was performed for 3 min (OPN4-mGluR1a) or 5 min (OPN4-mGluR1b, mCherry) with 965 nm laser at a framerate of 1,374 Hz. Responding Purkinje neurons were divided into 3 compartments consisting of distal dendrites, proximal dendrites, and soma region. Fluorescence levels of all regions for each neuron were analyzed using ImageJ *Time Series Analyzer V3* Plugin and normalized to their respective maximum fluorescence peak. For soma analysis all respective fluorescence levels of each group were normalized and averaged over time and maximum fluorescent changes determined.

Extracellular *in vivo* electrophysiological recordings in anaesthetized mice

For extracellular *in vivo* recordings anaesthetized mice were placed into a stereotaxic frame. After incision, a craniotomy above virus injection sites was made, and the dura removed. Using the Eckhorn system (Thomas Recording, Giessen, Germany) extracellular activity was recorded with up to six electrodes (impedance 2–3 MOhm at 1 kHz; Thomas Recording, Giessen, Germany), amplified and band-pass filtered at 0.1–8 kHz using a multichannel signal conditioner (CyerAmp380, Axon Instruments, Union City, CA, USA). Signals were sampled with 32 kHz (NI PCI-6259, National Instruments, Austin, TX, USA) controlled and offline analyzed using MATLAB. For optogenetic stimulation, a glass fiber was integrated in the multi-electrode system. Then, using 465 nm LED (Plexon, Dallas, USA) with 1.5–2 mW at the tip of the fibre pulses of different length were delivered. For pharmacological experiments, a micropipette was inserted in the multielectrode system (replacing the light fiber) and 200 μM DHPG (Abcam) was locally applied by pressure injection.

Immunohistochemistry

Mice were anesthetized and intracardially perfused using phosphate buffered saline (PBS) and 4% paraformaldehyde in phosphate buffer (PFA). Brains were removed, post-fixed overnight using PFA and cryoprotected in PBS with 30% sucrose (w/v) for at least 24 h. Sagittal slices of 35–40 μm were cut (CM3050 S, Leica), washed in 1xPBS, permeabilized 1 h with 0.3 PBS-Triton X-100 (PBST) and blocked using 10% normal donkey serum (NDS). Primary antibodies (rabbit anti mGluR1a, Sigma-Aldrich, 1:100) were applied overnight in 3% NDS in 0.3% PBST. After washing, slices were incubated in goat anti-rabbit antibody

conjugated with Alexa Fluor 488 (1:500, Invitrogen) for 3 h. Sections were mounted using Mowiol with DABCO. Images were collected using either a confocal (TC5 SP5, Leica) or 2P microscope (Ultima 2Pplus, Bruker).

Behavioral paradigms

Rotarod. Motor coordination and learning was assessed using an accelerated rotarod protocol. Rotation was set to accelerate from 4 to 40 rpm in 10 second increments. Mice were placed on a continuously rotating cylinder of 4 rpm constant speed. For Fos-TRAP experiments, training sessions consisted of 9 trials on day 1 and 2. For optogenetic experiments, mice were connected to glass fiber cables for optogenetic stimulation (PlexBright LED system, Campden Instruments, UK) and placed on the rod (at 4 rpm speed). Test and the light stimulation started as soon as a mouse was stable on the rod. Mice were trained on two consecutive days (D1 and D2) with light stimulation starting at the second trial. The session on D1 consisted of 9 trials, sessions on day 2 and 8 consisted of 11 trials (3 min intertrial interval). As soon as the mouse fell off the rod the light stimulation was stopped and latency to fall was determined. Offline, we analyzed the learning rate of every training day (adapted from[76];((mean latency to fall$_{last\ two\ trials}$) – (mean latency to fall$_{first\ two\ trials}$))/number of intertrial intervals).

Behavioral labeling using 4-hydrotamoxifen

Drug preparation. 4-hydroxytamoxifen (4-OHT) was prepared according to.[77] 10 mg of 4-OHT was dissolved in 250 μL DMSO, and 5 mL of saline with 2% Tween 80. The final solution entailed 20 mg/kg 4-OHT and was administered IP to Fos-TRAP animals at indicated timepoints according to their weight. Mice were injected 30 min after the training (indicated in Figure 4) and sacrificed 10 days later. After cryo-sectioning and mounting, Purkinje cells were visually identified by their location and soma diameter and counted throughout the cerebellum using THUNDER imaging system (Leica). tdTomato$^+$ PCs of the cerebellar areas were normalized to the summed tdTomato$^+$ PCs expression of the individual mice divided by the number of investigated areas.

QUANTIFICATION AND STATISTICAL ANALYSIS

Data are shown as mean ± standard error, as noted in each figure. n values are provided in the figure legends. Tests were performed with MATLAB or Sigma Plot (Systat software). For comparison between two independent groups, two-tailed Student's t-test, Mann-Whitney U test, Wilcoxon signed-rank test or Kolmogorov-Smirnov test were performed. For comparison between more than three groups, two-way analysis of variance (ANOVA) or Kruskal-Wallis tests with subsequent post hoc tests for detailed comparisons were employed. Statistical p-values of $p < 0.05$ were considered significant.